Electronic Supplementary Material (ESI) for Nanoscale.

Universal Discoidal Nano Platform for Intracellular Delivery of PNAs

Armin Tahmasbi Rad [a,b,*], Shipra Malik [c,*], Lin Yang [d], Tripat Kaur Oberoi-Khanuja [e], Mu-Ping Nieh [a,b,f,‡], Raman Bahal [c,‡]

Supporting Information

Fig. S1

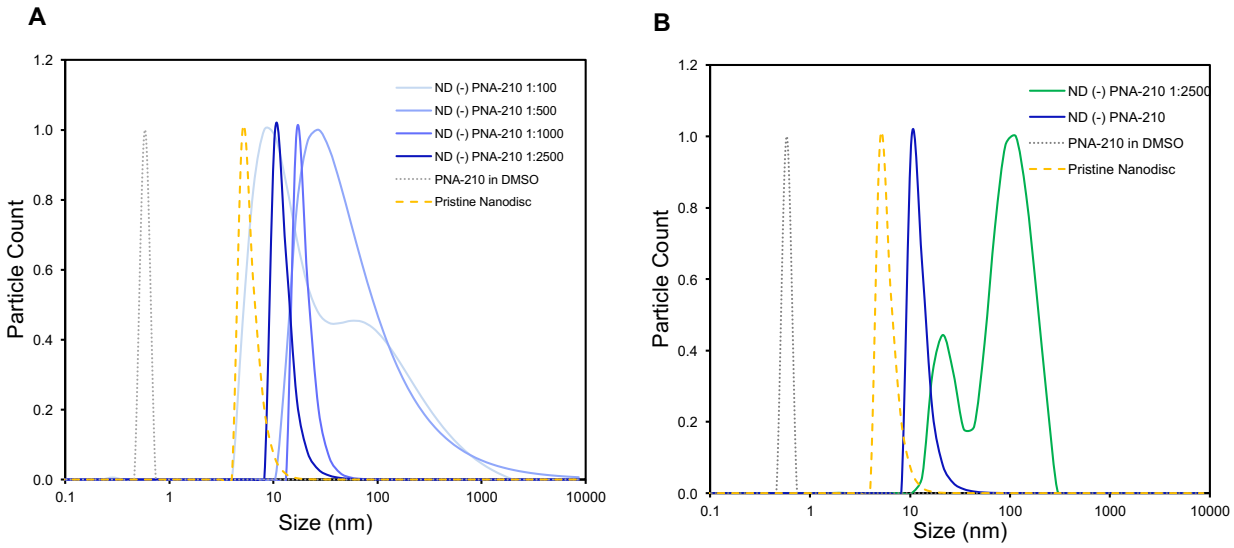

Fig. S1: (**A and B**) Size distribution of nanodiscs (ND) and nanovesicles containing antimiR-210 PNAs in the presence (solid) and absence (dotted) folate ligand

Fig. S2

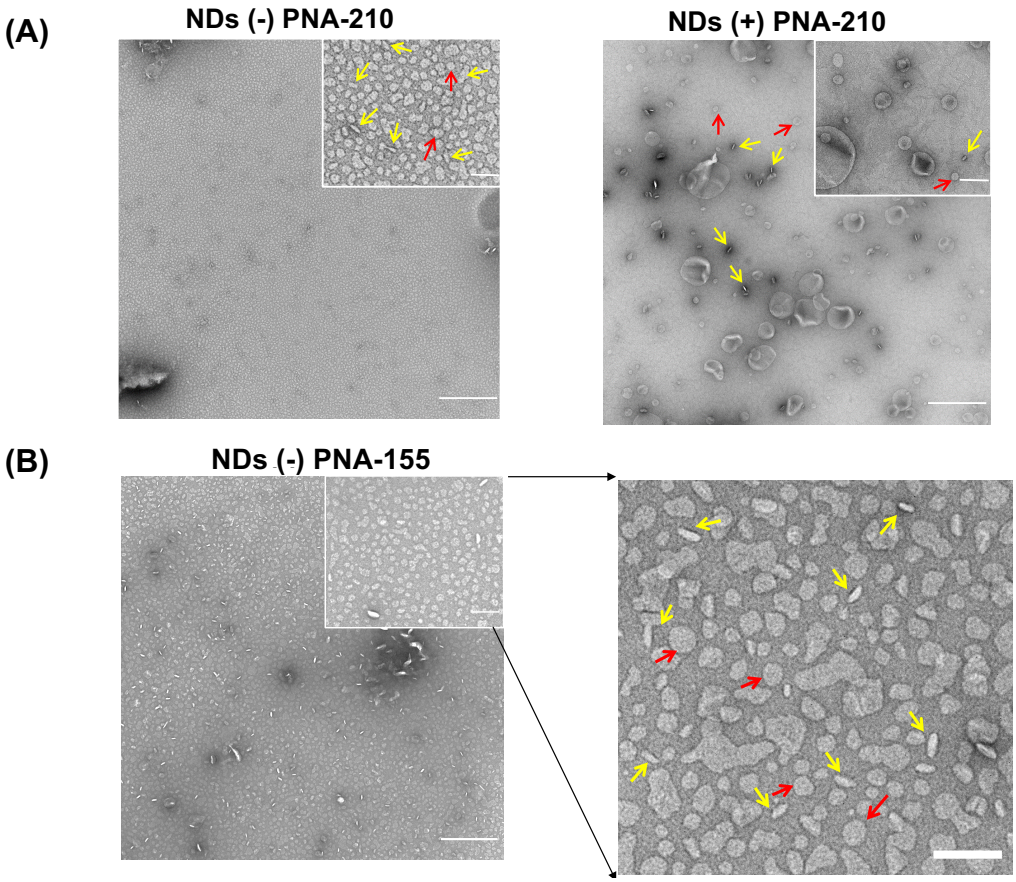

Fig S2. (**A**) TEM image of ND (-) and (+) encapsulating lipid:PNA molar ratio of 1:2500 loaded with PNA-210 and (**B**) ND (-) encapsulating lipid:PNA molar ratio of 1:2500 loaded with PNA-155. As shown, the shape and size is similar to (Fig 1B), which belongs to PNA-210. The planar and rim views are pointed by yellow and red arrows, respectively.

Fig S3

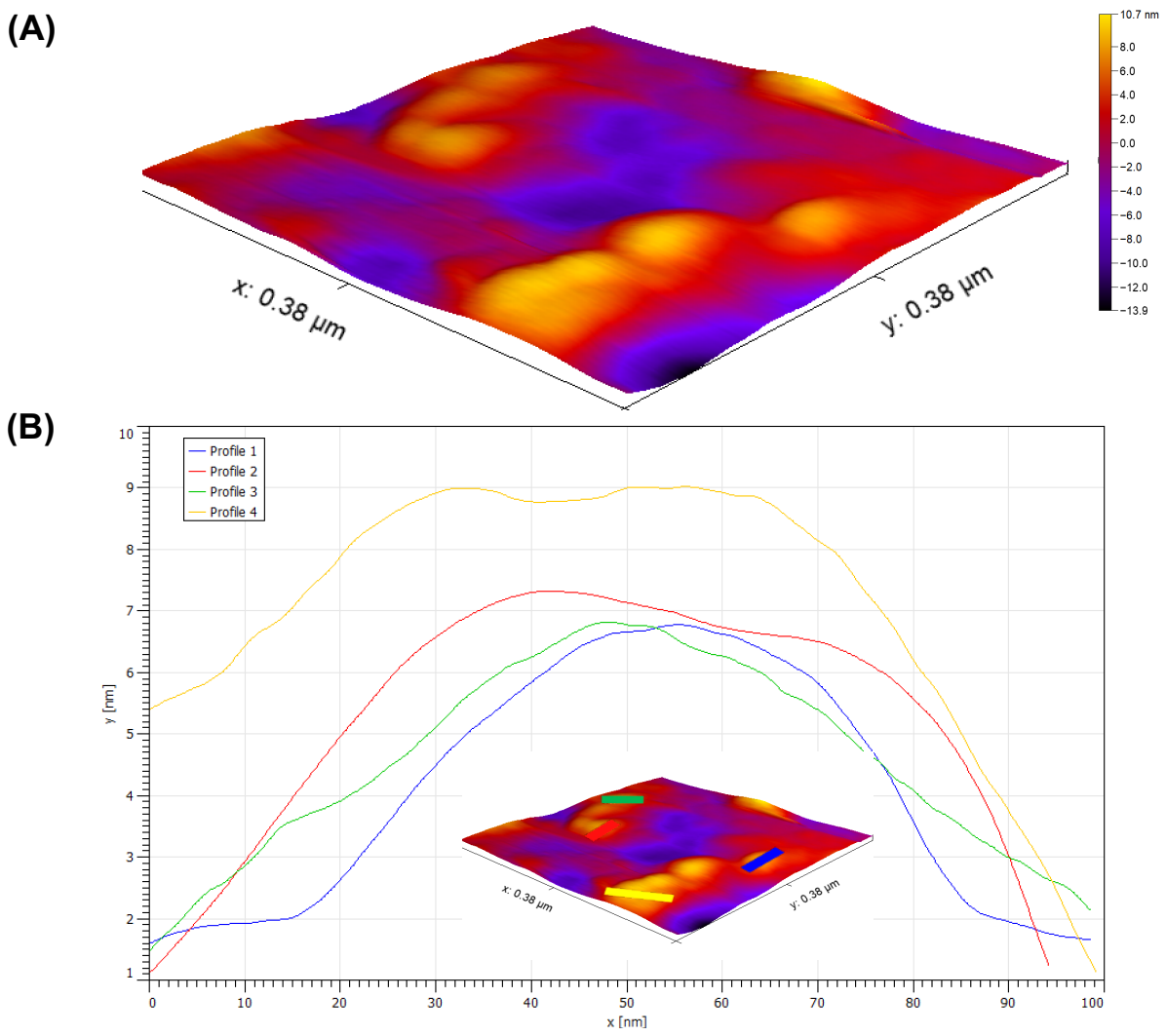

Fig S3. (**A**) Contact mode AFM images of dried specimen of ND (-) PNA155 1:2500 sample. The diameters of the NDs is consistent with the TEM images and the height profile is also measure and shown in part B. (**B**) Height profiles were obtained across the bicelles through figure (a). The inset shows the corresponding profile location in the image. As shown, the plateau height peak is expected for the discoidal shape.

Fig S4

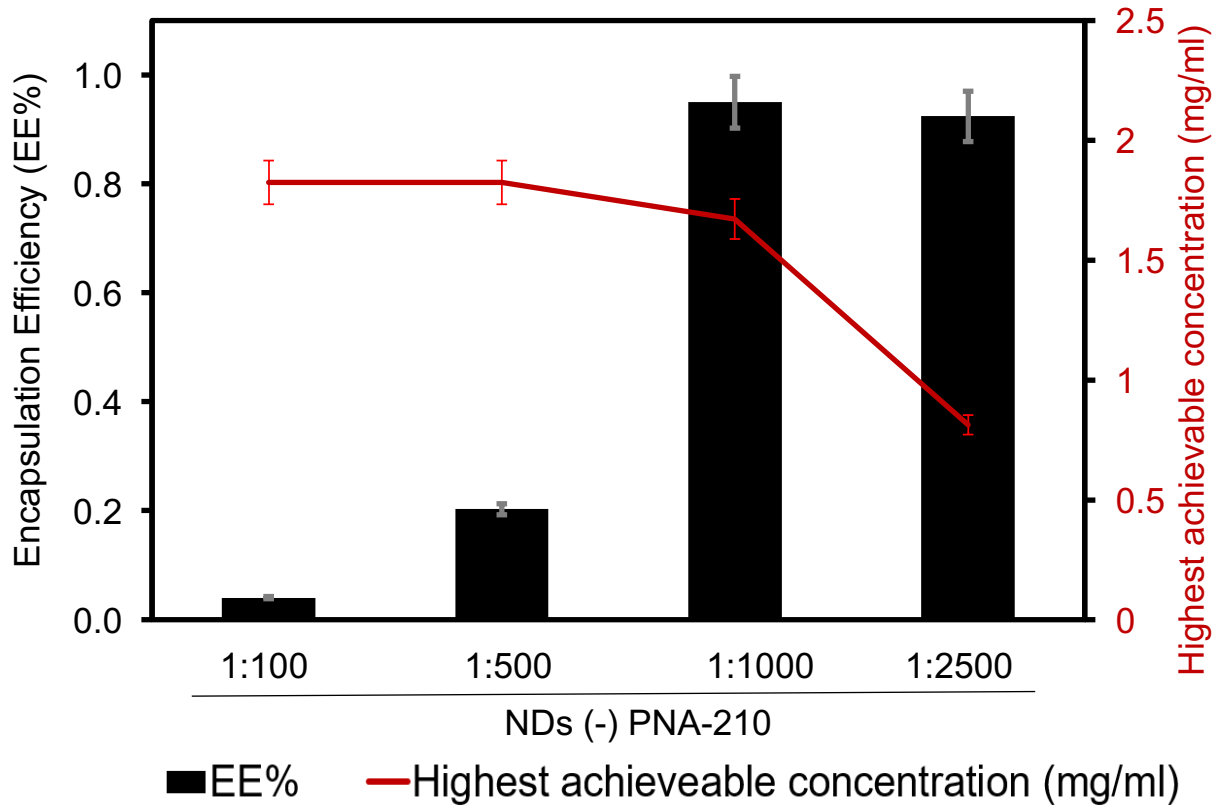

Fig. S4: Encapsulation Efficiencies of antimiR-210 PNA encapsulated in negative charge containing NDs with different PNA:lipid molar ratios. By decreasing the PNA content from 1:100 down to 1:2500 ratio, the encapsulation rate can be increased from less than 5% up to ~100%. The bar chart shows the encapsulation rates calculated by the ratio of encapsulated PNA molecules compared to the initial mass of added PNAs. However, as the line chart (left y-axis) shows, the highest achievable concentration of the PNAs encapsulated in NDs is decreased even though the EE is enhanced by lowering the lipid:PNA ratio.

Fig S5

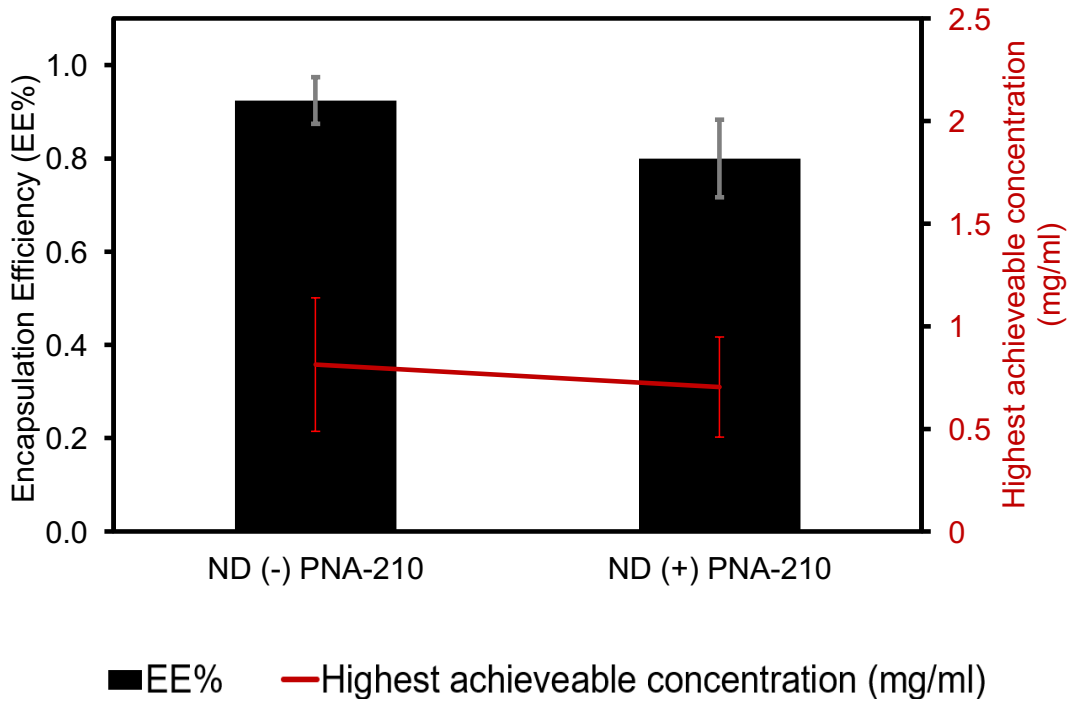

Fig. S5. Encapsulation Efficiencies of antimiR-210 PNA encapsulated in negatively and positively charged containing NDs. The bar chart shows the encapsulation rates calculated by the ratio of encapsulated PNA molecules compared to the initial mass of added PNAs. The line chart (left y-axis) indicates the highest achievable concentration of the PNAs encapsulated in NDs and stable in the aqueous phase. Although the TEM and SAXS confirmed that there are polydispersed mixture of bicelles and liposomes in the positive lipids, the encapsulation efficacy is not affected and it is still above 90%.

Fig S6

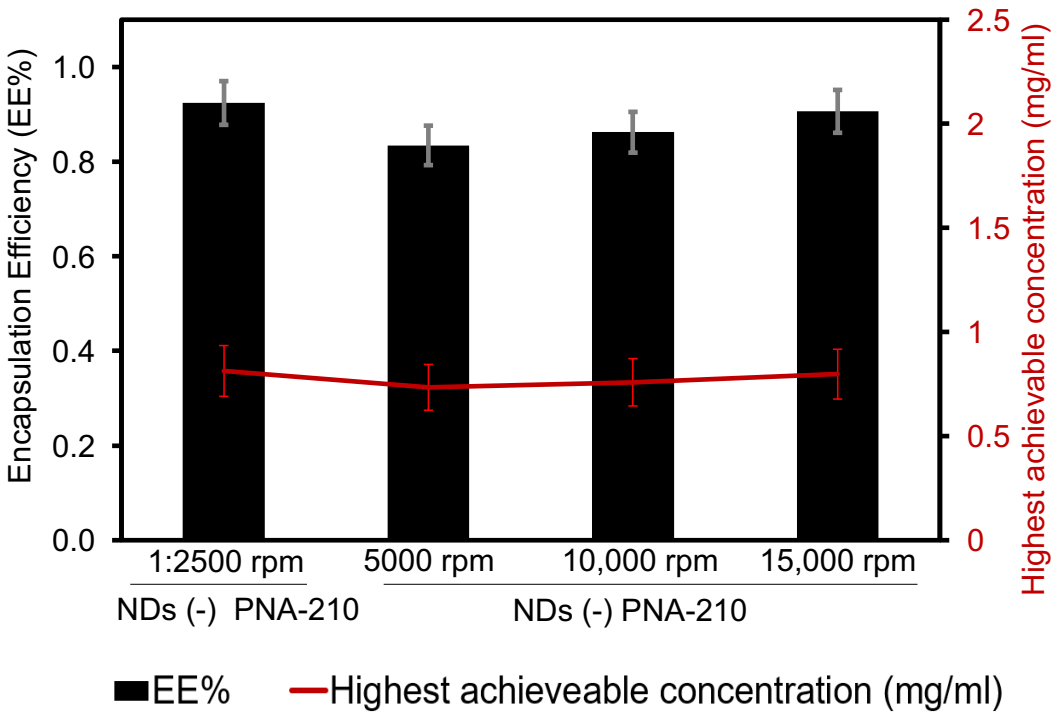

Fig. S6: Encapsulation Efficiencies of antimiR-210 PNAs encapsulated in negative charge containing NDs after centrifuging at different rates.

Fig S7

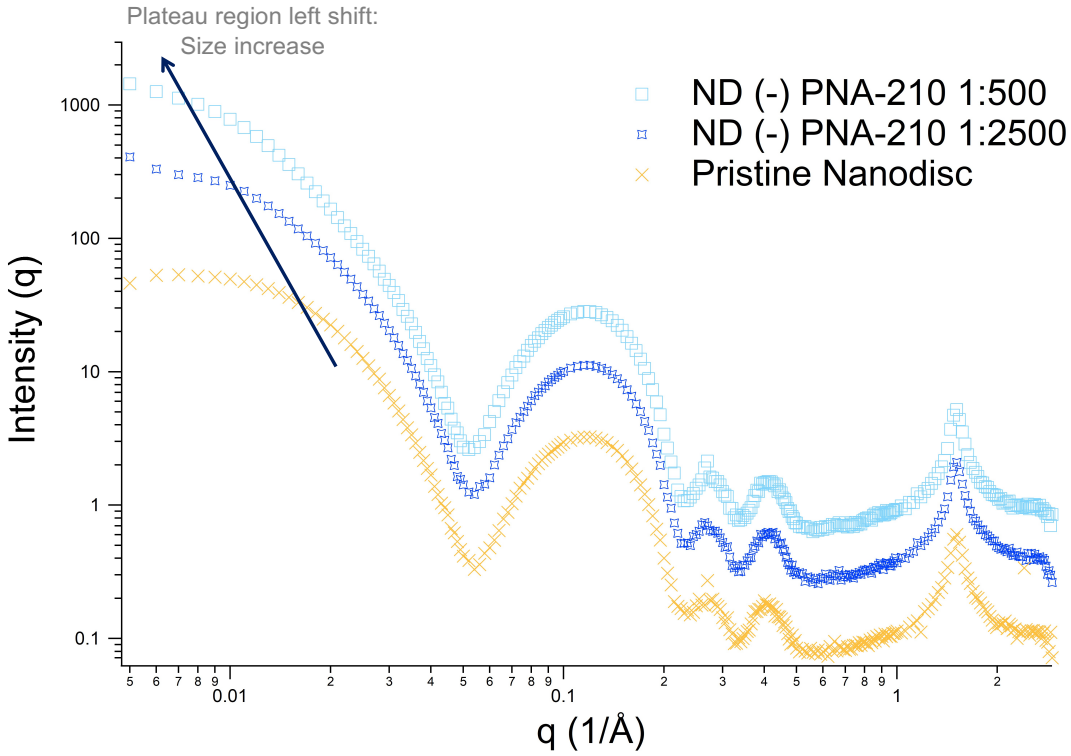

Fig S7. SAXS results of antimiR-210 PNAs encapsulated in negative NDs. All the curves start with the Guinier region which reciprocally correlates with the size of the nanocarriers. As shown by the navy arrow, the platue region shifts from ~0.015 to 0.005 1/Å which confirms the size increase due to the higher encapsulations.

Fig S8

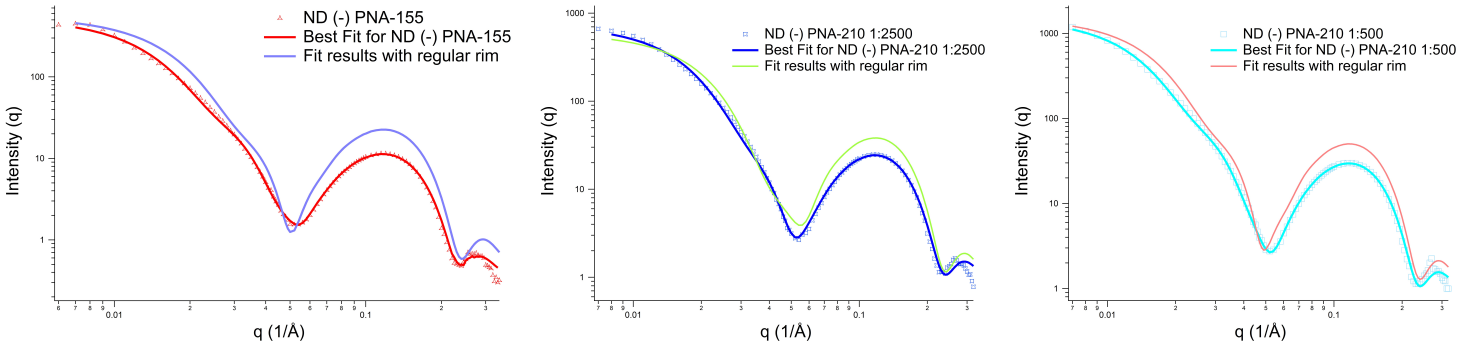

Fig S8. SAXS results of antimiR-PNAs encapsulated in NDs with the best fitting results plotted versus the fitting results with a fixed rim thickness value . As it can be observed, here the rim thicknesses play a major role in the final results and therefore the observed rim thickness expansion phenomena can be confirmed through this fitting studies.

Fig S9

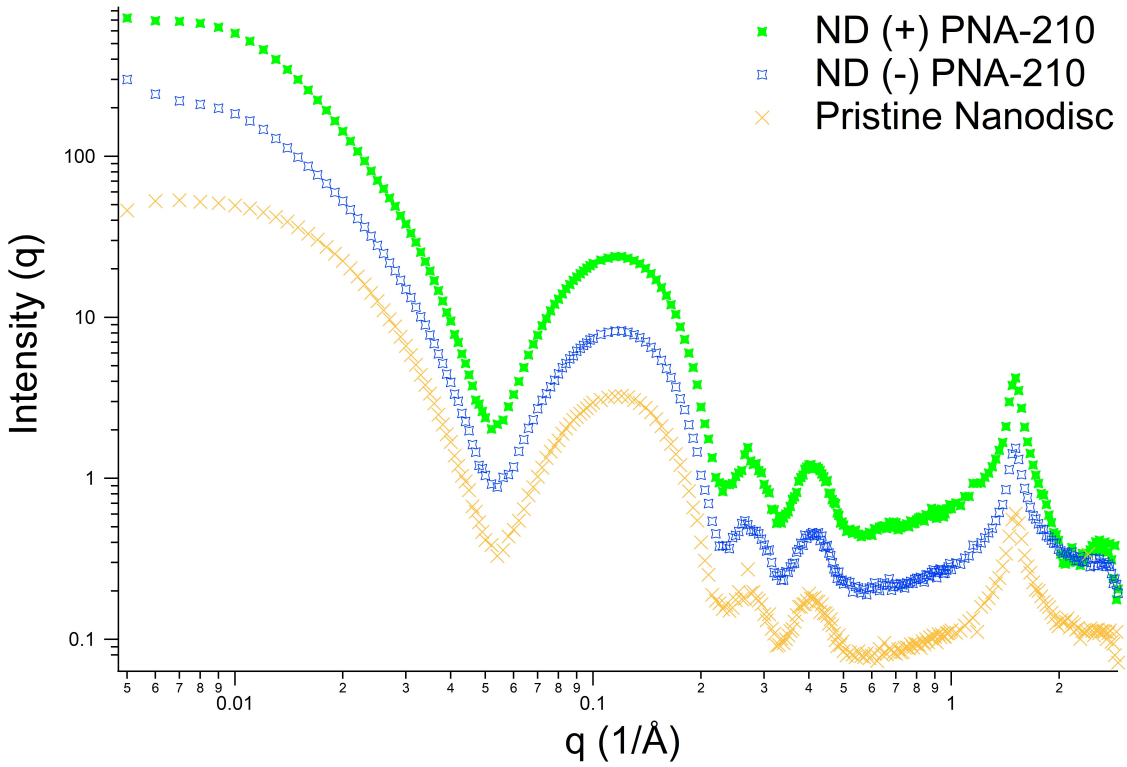

Fig S9. SAXS results of antimiR-210 PNAs encapsulated in negative and positive NDs.

Fig S10

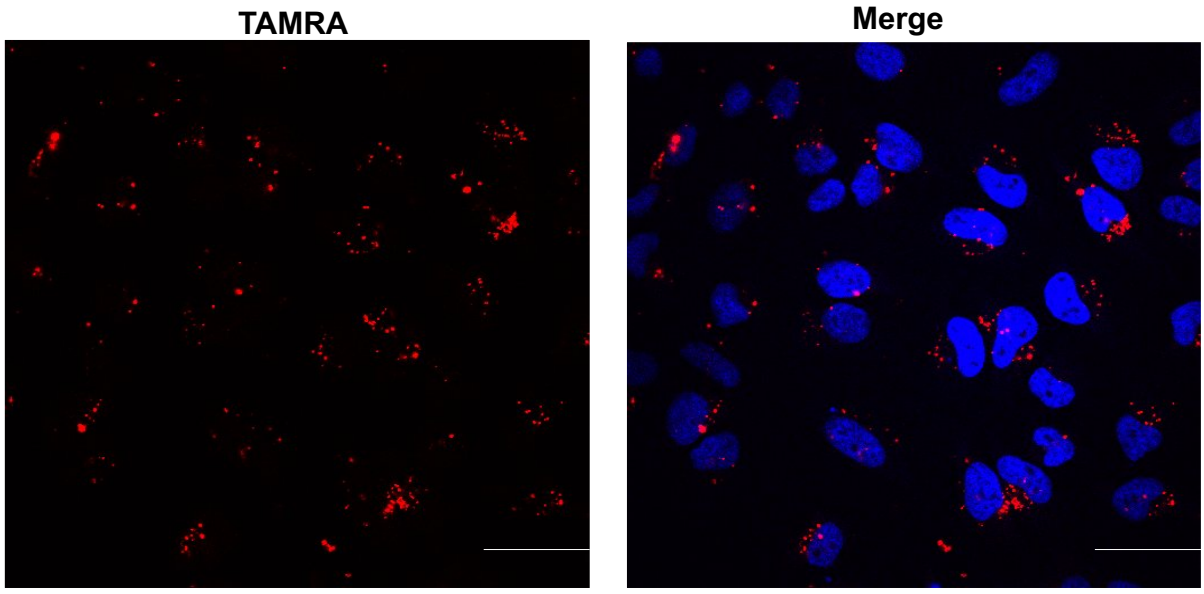

Fig S10. Fluorescent images of HeLa cells incubated with PLGA NPs containing antimIr-155 for 24 h, followed by brief washing with PBS and incubation with DAPI (Nuclear staining). Blue: nucleus (DAPI), red: PS oligomers (TAMRA).

Fig S11

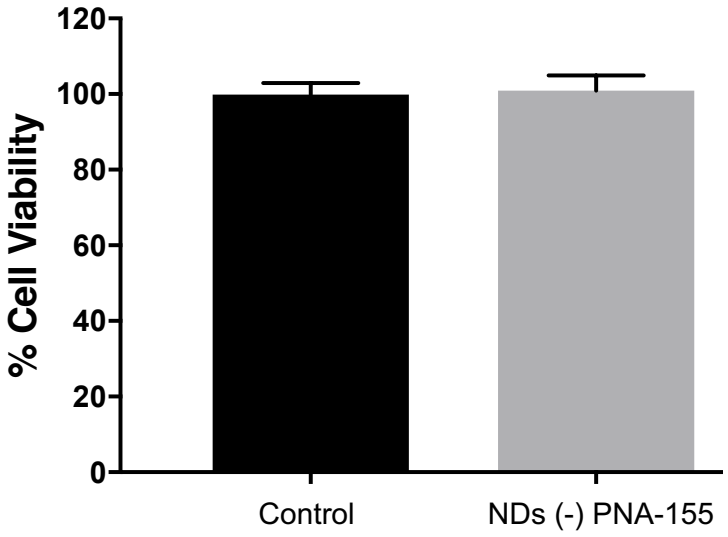

Fig S11. Safety profile studies on primary HEK293 cells. MTT assays were performed onto HEK293 cells treated with ND (-) PNA-155 as indicated on x axis at 24 h post treatment. N=6 samples were used and data are shown as mean ± s.d.

Fig S12

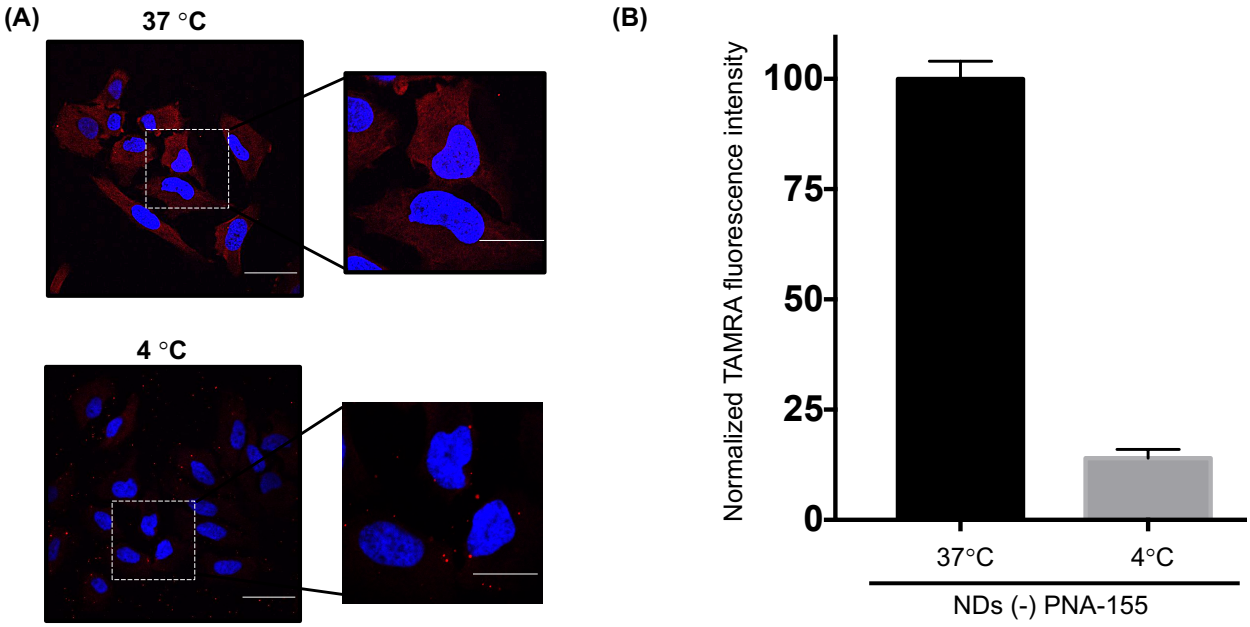

Fig S12. (A) Fluorescent images of HeLa cells incubated with NDs containing antimir-155 for 24 h at 37°C and 4°C, followed by brief washing with PBS and incubation with DAPI (nuclear staining). Blue: nucleus (DAPI), red: PNA oligomers (TAMRA).**(B)** FACS analysis of HeLa cells following incubation with the negative ND (-) containing PNA-155. 5000 cells were selected for the number of events. Data are shown as mean ± s.d.

Fig. S13

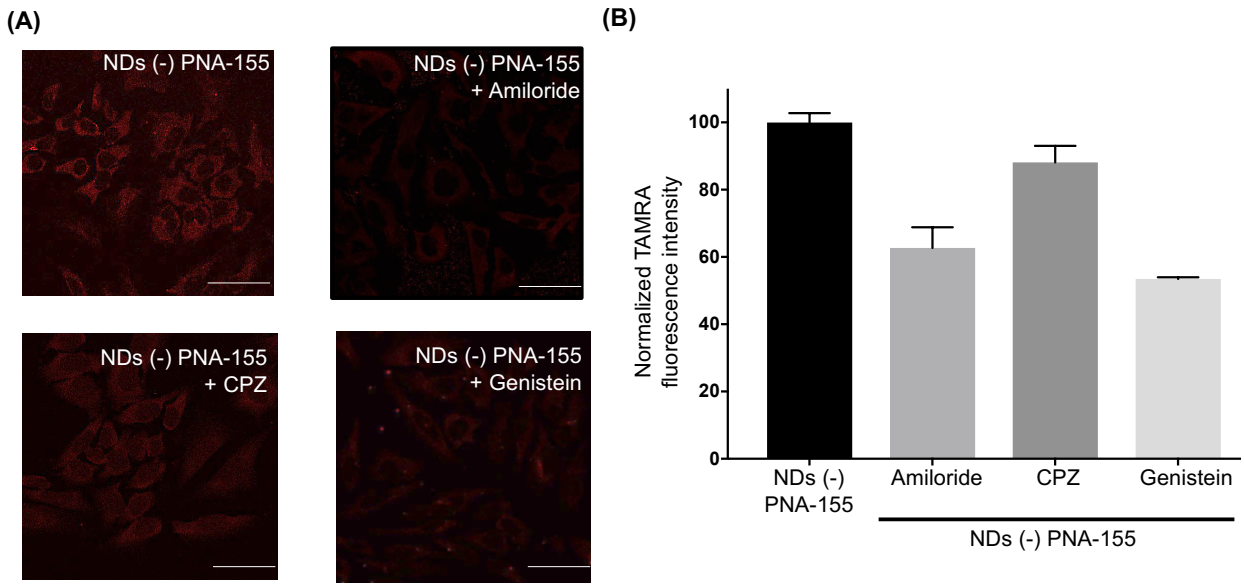

Fig S13. (A) Fluorescent images of HeLa cells incubated with NDs containing antimir-155 in the presence of endocytic inhibitors at 37^{o}C, followed by brief washing with PBS. Red: PNA oligomers (TAMRA). (B) FACS analysis of HeLa cells following incubation with the inhibitors and negative ND (-) containing PNA-155. Median fluorescence were calculated. 7500 cells were selected for the number of events. N=3 samples were used and data are shown as mean ± s.d.

Fig S14

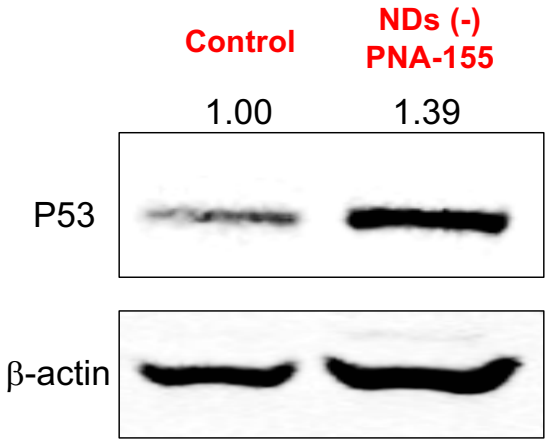

Fig S14. Western blots showing the levels of p53 protein in NDs (-) PNA-155 treated HeLa cells as compared to control.

Table 1. The encapsulation efficiencies described the encapsulated mass of PNA per mg of lipid in bicelles. Data was presented as n=3 for each sample.

Sample	OD (260 nm)	Concentration of encapsulated PNA (μg/ml)	Encapsulation efficiency (%) ± SD	Encapsulated PNAs (nmole/mg of lipid)
ND (-) PNA-210 1:2500	0.15 ± 0.01	0.41 ± 0.03	92 ± 7	0.72 ± 0.05
ND (-) PNA-210 1:1000	0.30 ± 0.02	0.84± 0.06	76 ± 6	1.48 ± 0.11
ND (-) PNA-210 1:500	0.33 ± 0.02	0.91± 0.05	42 ± 5	1.61 ± 0.19
ND (-) PNA-210 1:100	0.30 ± 0.01	0.84 ± 0.02	8 ± 3	1.47 ± 0.48
ND (+) PNA-210 1:2500	0.14 ± 0.01	0.39 ± 0.02	88 ± 7	0.66 ± 0.05
ND (-) PNA-155 1:2500	0.13 ± 0.01	0.38 ± 0.03	98 ± 7	0.57 ± 0.04